
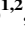








# Shallow Moonquake Mechanisms Illuminated by Rheologic Characteristics of Basaltic Gouges

Fengshou Zhang<sup>1,2</sup> , Wenzhi Zhao<sup>1,2</sup> , Mengke An<sup>1,2</sup> , Xianda Shen<sup>1,2</sup> , Jizhou Tang<sup>3</sup> ,  
Luanxiao Zhao<sup>3</sup> , Hai Liu<sup>4</sup> , Derek Elsworth<sup>5,6</sup> , Hehua Zhu<sup>1,2</sup>, and Manchao He<sup>7</sup>

<sup>1</sup>Department of Geotechnical Engineering, College of Civil Engineering, Tongji University, Shanghai, China, <sup>2</sup>Key Laboratory of Geotechnical and Underground Engineering of Ministry of Education, Tongji University, Shanghai, China, <sup>3</sup>State Key Laboratory of Marine Geology, Tongji University, Shanghai, China, <sup>4</sup>School of Civil Engineering, Guangzhou University, Guangzhou, China, <sup>5</sup>Department of Energy and Mineral Engineering, EMS Energy Institute and G3 Center, the Pennsylvania State University, University Park, PA, USA, <sup>6</sup>Department of Geosciences, the Pennsylvania State University, University Park, PA, USA, <sup>7</sup>State Key Laboratory for Geomechanics and Deep Underground Engineering, China University of Mining and Technology, Beijing, China

### Key Points:

- Moonquakes throughout the crust are consistent with the v-weakening characteristics of gouge at intermediate stresses and temperatures
- Rheological heterogeneity of mineral fragments is a potential cause of unstable sliding on faults
- Stress transfer and accumulation is an important candidate to explain the generation of shallow moonquakes

### Supporting Information:

Supporting Information may be found in the online version of this article.

### Correspondence to:

M. An,  
2015mengkean@tongji.edu.cn

### Citation:

Zhang, F., Zhao, W., An, M., Shen, X., Tang, J., Zhao, L., et al. (2024). Shallow moonquake mechanisms illuminated by rheologic characteristics of basaltic gouges. *Journal of Geophysical Research: Planets*, 129, e2024JE008370. <https://doi.org/10.1029/2024JE008370>

Received 29 FEB 2024

Accepted 28 OCT 2024

**Abstract** The projected evolutionary history of the Moon and observed occurrence of moonquakes suggest that brittle faulting is present in the shallow lunar crust. The main component of the lunar crust, plagioclase, shows velocity-strengthening behavior in the range of crustal temperatures. Chang'e 5 samples of lunar regolith show a mineral composition almost identical to basaltic bedrock. We measured the friction-stability characteristics of dry synthetic gouges representative of basaltic faults assumed to be present in the lunar crust. Frictional strengths are  $\sim 0.7$  and exhibit an overall velocity-strengthening response but transition to velocity-weakening at intermediate temperatures ( $\sim 200$ – $300^\circ\text{C}$ ) and stresses ( $\sim 25$ – $100$  MPa). Bounding temperature profiles representative of the lunar crust suggest that moonquakes are feasible in the lunar crust. The rheological heterogeneity of mineral fragments in basalt is a potential cause of unstable sliding on faults with the related steady-state stress drop close to the minimum of the estimated dynamic stress drop. This suggests that some events with small stress drops are associated with the instability of mature basalt faults. However, observations of shallow moonquakes with high stress drop but merely moderate magnitude suggest that high degrees of healing on immature faults, small seismic nucleation lengths, or the failure of intact crust are present. We emphasize that moonquakes may arise from stress transfer and accumulation due to processes such as cooling contraction.

**Plain Language Summary** Shallow moonquakes have similar characteristics to earthquakes. However, their sparsity and uncharacteristically large duration compared to terrestrial earthquakes and on a planet lacking large-scale tectonics make the mechanisms enigmatic. We explore the mechanism of shallow moonquakes from the perspective of laboratory faults using synthetic samples replicating those recovered from the Chang'e-5 mission. Regolith samples suggest that they are derived from a basaltic crust. We measure the frictional strength and whether rheology is either ductile or brittle – the latter being a prerequisite for moonquakes. We find that brittle failure may indeed occur in the lunar crust and that the stress drop under steady-state sliding is close to the minimum of the reported dynamic stress drop. Stress drops are large but return only moderate seismic magnitudes. Given limits on observed strengths of the fault gouge – these remain enigmatic. We propose that the healing and strengthening of young faults, the rupture of intact crust, or the absence of large-scale faults are prerequisites to explain this anomalous behavior.

## 1. Introduction

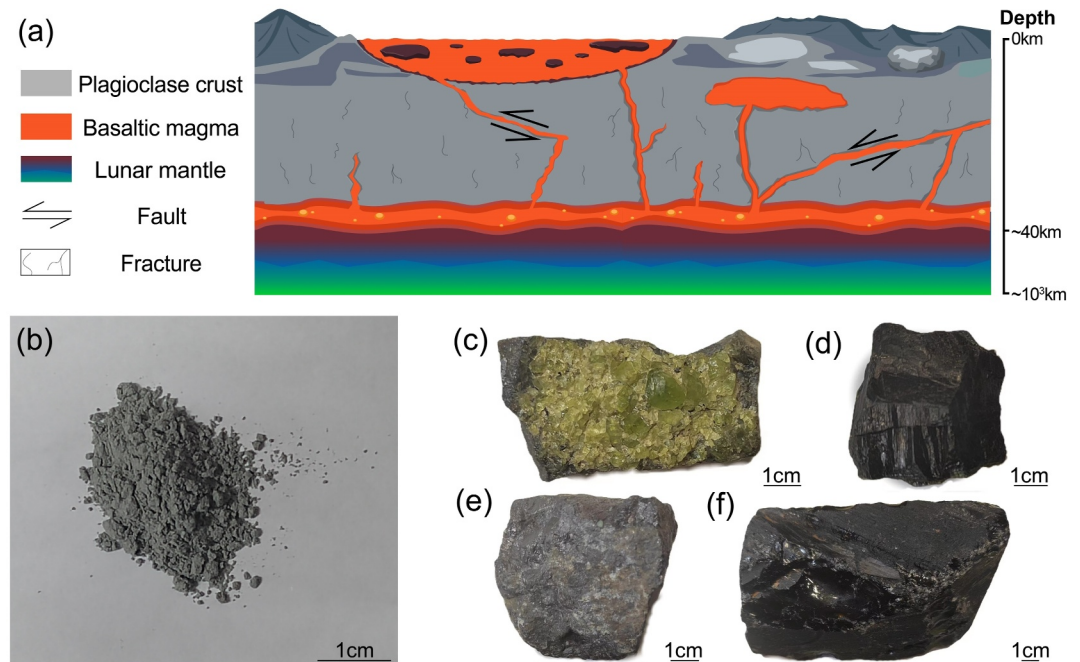
Lunar exploration has advanced and will further advance our understanding of planetary evolution and that of the inner solar system (Crawford & Joy, 2014). Lunar missions encompassing remote sensing, surface exploration, and sample return contribute to an improved understanding of the internal composition of the Moon and give rise to the concept of the Lunar Magma Ocean (LMO) (Wieczorek et al., 2006). The LMO model explains the presence of the Moon's largely anorthositic crust, basalt source and the presence of KREEP elements - incompatible elements enriched in remnant magma, with Potassium (K), Rare Earth Elements (REEs) and Phosphorus (P) being the dominant elements (Moriarty et al., 2021). Observations of lunar seismicity have provided valuable information in understanding the interior structure of the Moon since the United States conducted several seismic

experiments during the 1969–1977 Apollo landings (Nakamura et al., 1982). Data on moonquakes derived from the Apollo projects indicate the existence of deep, shallow, impact and a significant fraction of unclassified moonquakes (Nunn et al., 2020). A strong correlation is evident between deep moonquakes and tidal forcing driven by the Earth-Moon cycle (Kawamura et al., 2017; Weber et al., 2009). Some shallow moonquakes are likely to be associated with tidal effect or impact events, with their hypocenters locatable but with large uncertainties (Gagnepain-Beyneix et al., 2006; Garcia et al., 2011; Gillet et al., 2017; Khan et al., 2006; Lammlein, 1977; Lognonné et al., 2003). Uncharacteristically, the strong scattering of lunar seismic waves can cause shallow moonquakes to last for up to an hour, unlike terrestrial earthquakes that last a few minutes and slow-slip events that last several days or more (Ito et al., 2007; Nakamura et al., 1982). Notably, shallow moonquakes are the most energetic radiation sources to the lunar surface compared with other moonquakes (Nakamura et al., 1982), suggesting potentially brittle failure mechanisms. Their signals are most detectable as teleseismic sources and would be the most hazardous for any habitation on the lunar surface. The similarity of various features of moonquakes and intraplate earthquakes also suggests that they may have similar origins and occur in locations with structural weaknesses (Nakamura, 1980).

Several possible causes of moonquakes have been proposed, such as quark matter from unknown sources (Frohlich & Nakamura, 2006), geochemical differentiation and thermal effects near a basin (Nakamura et al., 1979). Recently, Watters et al. (2019) proposed that brittle failure induced by cooling shrinkage may be the source of shallow moonquakes based on the assumption that these events are related to the coseismic slip of faults. However, an instability criterion has not yet been validated, which may result in the predicted depths of shallow moonquakes being imprecise. Thus, the causal mechanisms of shallow moonquakes remain poorly understood, and laboratory evidence is missing. Fault gouge is highly comminuted wall rock residing within the fault and sourced from the host rock due to fault rupture and slip with particles typically <2 mm in diameter. For mature faults, slip is localized in the fault gouge as it is the weakest component of the fault (Bedford et al., 2022; Ikari et al., 2011) and its frictional stability determines whether faults are able to accelerate from subseismic to seismic velocities. The first step in inferring the frictional properties of lunar crust faults is to analyze their possible mineralogical composition of the faults. The LMO model describes the early Moon as capped by a floating plagioclase crust, with the present anorthosite highlands associated with this early plagioclase flotation (Moriarty et al., 2021). Decompression melting of the lunar mantle results in intrusion into the lunar crust that potentially reaches the surface (Figure 1a) (Beard et al., 1998; Head & Wilson, 2017; Wilson & Head, 2017). Thus, the frictional properties of the two rocks (anorthosite and basalt) comprising the faults will control the slip behaviors of mature faults.

Early analyses of seismic data indicate that the lunar crust may be aseismic (Nakamura et al., 1979). This conclusion may be consistent with the velocity-strengthening behavior exhibited by the plagioclase gouge under dry conditions in the temperature range of 100°C–600°C. Experimental results show that the evolution effect is negligible, allowing velocity-strengthening behavior across this full range of temperatures (He et al., 2016). Another phenomenon that suggests that anorthosite faults are aseismic, but is inconclusive, is that lunar crust with a porosity of 12% may have numerous faults and fractures but produces only 4–5 shallow moonquakes annually, much fewer than deep and impact moonquakes (Nakamura, 1980; Wieczorek et al., 2013). However, relocations show that the depths of some events are shallower than 30 km within the lunar crust, which is ~34–43 km thick (Figure S1 in Supporting Information S1) (Wieczorek et al., 2013). Furthermore, lobate scarps on the surface suggest that shallow moonquakes may be linked to coseismic slip on surface faults (Watters et al., 2019). Observed scarps are surface traces of faults and may be the origin of shallow moonquakes driven by underlying basaltic faults. These observations, therefore, suggest that the shallow moonquakes may be associated with unstable sliding on faults in the basalt – and thus, a question arises as to the controls of this instability.

Shear experiments on fault gouges are able to define this potential instability and therefore contribute to defining the feasibility of this mechanism for moonquakes (Frye & Marone, 2002; Giacomel et al., 2021; Ikari et al., 2020; Marone et al., 1990; Phillips et al., 2020; Zhang et al., 2017). The landing site of the Chang'e 5 mission occurs in the lunar maria, and the newly acquired in situ lunar regolith available from the recent Chang'e 5 mission is likely largely derived from the crust (Li et al., 2022). Retrieved samples have a mineral composition close to basaltic bedrock with the least contamination and are homologous to some of the Apollo mission samples (Li et al., 2022; Qian et al., 2021). We use synthetic fault gouges referenced to the Chang'e 5-recovered samples to measure frictional and stability properties representative of lunar faults in basalt (Figure 1b). Specifically, we focus on the impacts of stress and temperature on the frictional properties of the dry synthetic gouges to understand the



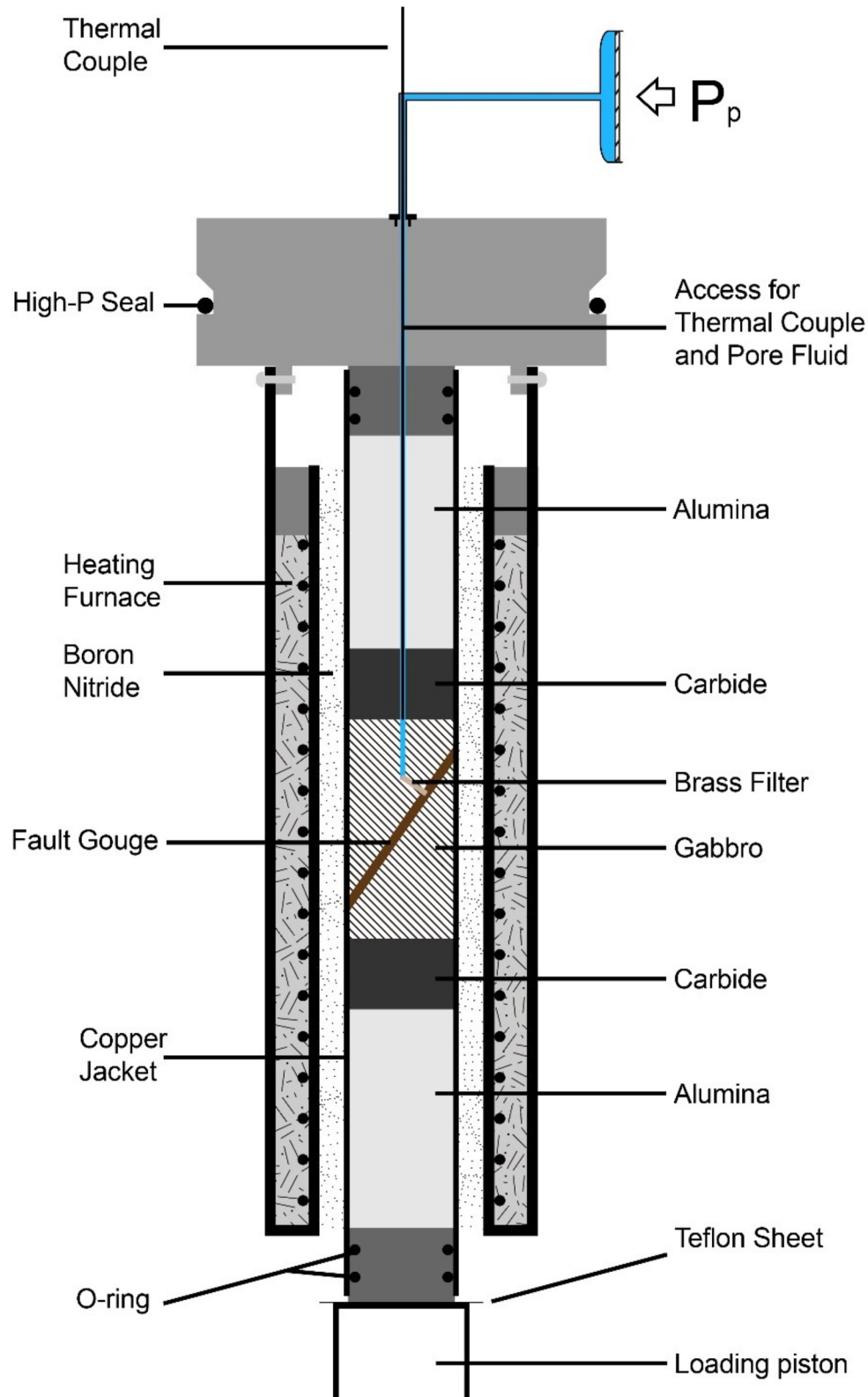
**Figure 1.** Schematic of lunar volcanism and synthetic fault gouge comprised from parent rock samples. (a) Crustal section showing modes of lunar volcanism. Chang'e 5 samples comprised basaltic magma recovered from the lunar surface. (b) Synthetic fault gouge (a photo under artificial light source) prepared from the homogeneous mixing of powders from several parent samples. (c) Olivine derived from olivine-bearing inclusions in basalt. (d) Hedenbergite (pyroxene). (e) Ilmenite with impurities. (f) Volcanic glass. XRD results for all rock powders are presented in Figure S2 in Supporting Information S1.

potential for creating moonquakes and to explain the cause of the anomalously high stress drop (up to 210 MPa) but moderate magnitude ( $M_b \approx 5$ ) of the shallow moonquakes observed in previous lunar seismic observations (Oberst, 1987). This work defines the seismic potential of the basaltic faults and has implications for the mechanisms controlling shallow moonquakes and the influence of the lunar temperature profile.

## 2. Material and Methods

The reference samples of synthetic gouges are three lunar soil samples (No. CE5C0800YJFM001-1, No. CE5C0100YJFM002-1, No. CE5C0100YJFM002-2) collected by the Chang'e 5 mission, which are weathering products of mare basalts (Li et al., 2022). Synthetic fault gouge was prepared by uniformly mixing the five minerals, pyroxene, plagioclase, ilmenite, olivine, and volcanic glass, prior to the experiments (Figures 1c–1f). The parent samples were ground to a final particle size of  $<75 \mu\text{m}$  (200 mesh) with a final mass fraction of gouge composition of 41.7 wt.% pyroxene, 29.8 wt.% plagioclase, 16.9 wt.% volcanic glass, 5.4 wt.% forsterite, 1.8 wt.% ilmenite and 4.4 wt.% other minerals (Figure S2 and Table S1 in Supporting Information S1). We then used a triaxial shearing apparatus in the Institute of Geology, China Earthquake Administration, to conduct all experiments (Figure 2). In these experiments, 1 mm thick synthetic fault gouges were sandwiched at  $35^\circ$  to the major principal-stress axis by two gabbro driving blocks. The simulated fault surfaces of the gabbro blocks were roughened by 200-mesh carborundum to eliminate boundary slip, with the initial sample area the same as the simulated fault surface at  $5.48 \text{ cm}^2$ . The upper block was drilled with a hole accommodating the pore pressures and a temperature sensor. Confining pressure was applied by filling the sealed vessel with argon gas after evacuating the internal gas. A piston rod coated with Teflon applied the shear force with the sample heated by a resistance heater.

Initial measurements suggest that the moisture content of the lunar magma is  $<0.165 \text{ wt.}\%$ , the cumulative moisture content of the magma remnants is less than  $1.4 \text{ wt.}\%$ , and the moisture contents of other sample minerals are even lower (Hui et al., 2013; Lin et al., 2017, 2022). The drying process in our experiments follows He et al. (2016). Temperatures from  $100^\circ\text{C}$  to  $450^\circ\text{C}$  were applied in our experiments, with faults stressed at 25 and



**Figure 2.** Schematic diagram of the structure inside the chamber of the triaxial device. The heating furnace and devices are placed in a hermetic chamber, sealed above by a high-pressure rubber ring, with the lower seal applied at the lower part of the piston. The hermetic chamber is pressurized by argon as a confining fluid, with the piston rod applying the axial stress. The upper fluid pathway is opened and connected to the atmosphere to fully evaporate the residual moisture when performing dry experiments. Data acquisition and other experimental details are described in Text S1 in Supporting Information S1.

100 MPa representing faults at 9.5 and 40 km below the lunar surface, respectively. We explored the influence of stress on the frictional properties of the fault gouges at a lower temperature of 100°C for comparison with terrestrial conditions. To understand the difference between basaltic faults on the Earth and the Moon, we also examined the influence of dry and wet conditions on fault stability (Table S2 in Supporting Information S1).

The initial shear velocity in the experiments is 1.22  $\mu\text{m/s}$  with the velocity steps progressing as 1.22–0.244 - 0.0488–0.244 - 1.22–0.244 - 0.0488  $\mu\text{m/s}$  in sequence, with the velocity dependence calculated using rate-and-state friction rheology. Rate-and-state friction (RSF) is a phenomenological law that describes second-order effects delimiting static and dynamic friction. It links the dependence of frictional resistance on slip velocity ( $V$ ) and an evolving state variable ( $\theta$ ). The frictional response of a fault varies with the previous loading history and depends on the direct effect ( $a$  parameter of the RSF), the evolution effect ( $b$  parameter of the RSF) and the gradual evolution of the sliding interfaces ( $D_c$  parameter of the RSF) (Dieterich, 1978; Ruina, 1983),

$$\mu = \mu_0 + a \ln\left(\frac{V}{V_0}\right) + b \ln\left(\frac{V_0\theta}{D_c}\right) \quad (1)$$

$$\frac{d\theta}{dt} = 1 - \frac{V\theta}{D_c} \quad (2)$$

where  $\mu_0$  is a constant appropriate for a steady-state slip at velocity  $V_0$ , and  $V$  is the frictional slip rate after the change in velocity when the friction coefficient is  $\mu$ .  $\theta$  is a state variable, with the change in the state variable  $\theta$  at a given time step ( $dt$ ) calculated from Equation 2 (Ruina, 1983), and  $a$  and  $b$  are empirical constants. For steady-state sliding,

$$a - b = \frac{\Delta\mu_{ss}}{\Delta \ln V} \quad (3)$$

with  $\Delta\mu_{ss}$  as the difference between the coefficient of friction before and after the velocity change under steady-state friction, with  $\Delta \ln V = \ln(V/V_0)$ . The RSF law was used to fit the coefficient of friction and the ( $a - b$ ) value to evaluate both the strength and evolution of the stability of the fault (Figure S3 in Supporting Information S1). Velocity strengthening ( $a - b > 0$ ) response indicates that slip will self-stabilize as frictional resistance increases with increasing velocity. In contrast, velocity weakening ( $a - b < 0$ ) may evolve into instability as resistance decreases with increasing slip velocity. Seismic nucleation will then only occur when the fault stiffness is larger than the system stiffness for velocity-weakening faults. RSF theory and iterative least squares methods were used to determine frictional constitutive parameters. The parameters were calculated by a Matlab-based script RSFit3000 (Skarbak & Savage, 2019). We chose the representative frictional coefficient at a shear displacement of 2.5 mm as the frictional strength of the simulated fault. Laboratory stress drop was calculated according to (Beeler et al., 2001),

$$\Delta\tau = |\Delta\mu_{ss}| \cdot \sigma_N \quad (4)$$

where  $\Delta\mu_{ss}$  was evaluated from Equation 3 and  $\sigma_N$  was evaluated from Equation S6 in Supporting Information S1. In order to compare the experimental data with the existing lunar models, we set gravitational acceleration representative of the Moon to 1.63  $\text{m/s}^2$ , and density of the lunar crust to 2,550  $\text{kg/m}^3$  within 1 km depth and 2,898  $\text{kg/m}^3$  between 1 and 60 km (Hirt & Featherstone, 2012; Zuber et al., 2013). The possible projected depth is obtained by dividing the effective normal stress by the gravitational acceleration and density.

After each experiment, we performed a microscopic analysis of the sample. To recover intact samples after testing, we retained a portion of the copper jacket on the outside of the driving block and dried it at 75°C for 48 hr. The samples were then impregnated with resin in a vacuum. After hardening, the resin-impregnated samples were sliced, polished, carbon-coated, and analyzed with a backscattered electron-scanning electron microscope (BSE-SEM) to define the microstructure. Elastic restraint from the copper jackets was corrected-out when analyzing the experimental results.

**Table 1**  
Frictional Properties and Fits for the Rate State Friction Law Parameters

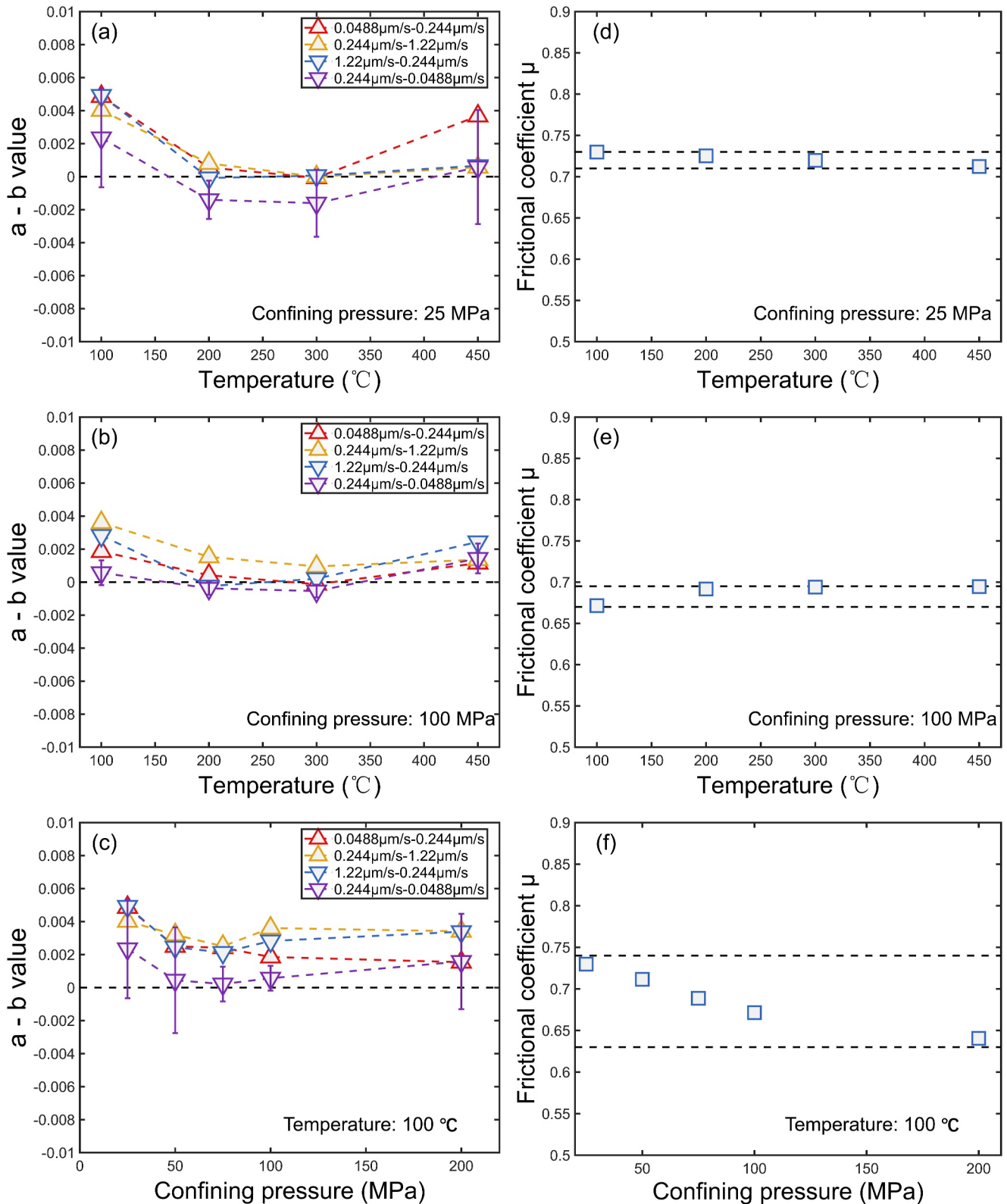
Serial number	RSF - $a$ value ( $\times 10^{-3}$ ) at velocity steps				RSF - $b$ value ( $\times 10^{-3}$ ) at velocity steps				RSF - $D_c$ value ( $\mu\text{m}$ ) at velocity steps				$\mu_{ss}$ ( $I_{disp} = 2.5 \text{ mm}$ )
	0.0488 $\mu\text{m/s}$	0.244 $\mu\text{m/s}$	1.22 $\mu\text{m/s}$	0.0488 $\mu\text{m/s}$	0.244 $\mu\text{m/s}$	1.22 $\mu\text{m/s}$	0.244 $\mu\text{m/s}$	0.0488 $\mu\text{m/s}$	0.0488 $\mu\text{m/s}$	0.244 $\mu\text{m/s}$	1.22 $\mu\text{m/s}$	0.244 $\mu\text{m/s}$	
CE5SIM-1	11.19	7.01	20.55	10.58 $\pm$ 1.52	6.33	2.99	15.63	8.24 $\pm$ 1.47	3.26	47.75	3.58	13.13 $\pm$ 3.45	0.7298
CE5SIM-2	18.29	5.99	5.66	5.01 $\pm$ 0.57	17.74	5.19	5.74	6.41 $\pm$ 0.59	0.27	1.91	11.01	8.16 $\pm$ 1.74	0.7252
CE5SIM-3	3.19	2.19	8.16	4.87 $\pm$ 1.43	3.26	2.19	8.1	6.48 $\pm$ 0.61	2.24	25.63	5.93	10.7 $\pm$ 0.74	0.7197
CE5SIM-4	9.05	3.42	11.56	9.86 $\pm$ 1.78	5.38	2.85	10.9	9.28 $\pm$ 1.68	2.71	1.93	2.43	8.03 $\pm$ 2.86	0.7123
CE5SIM-5	5.21	7.54	8.27	5.88 $\pm$ 0.49	3.35	3.93	5.44	5.31 $\pm$ 0.27	21.61	15.6	25.27	28.95 $\pm$ 4.45	0.6715
CE5SIM-6	3.81	4.35	3.14	3.08 $\pm$ 0.37	3.4	2.82	3.37	3.45 $\pm$ 0.02	5.2	5.79	31.29	22.76 $\pm$ 8.74	0.6917
CE5SIM-7	4.33	7.28	4.82	3.87 $\pm$ 0.38	4.46	6.32	4.62	4.41 $\pm$ 0.01	6.87	4.25	21.27	27.2 $\pm$ 1.22	0.6940
CE5SIM-8	8.45	12.18	6.22	6.01 $\pm$ 0.31	7.3	10.82	3.78	4.58 $\pm$ 0.59	6.92	2.68	30	67.08 $\pm$ 2.39	0.6946
CE5SIM-9	6.41	12.85	9.83	7.70 $\pm$ 2.86	3.91	9.65	7.38	7.25 $\pm$ 0.35	7.45	2.5	11.29	14.86 $\pm$ 4.60	0.7115
CE5SIM-10	7.85	6.7	7.63	5.72 $\pm$ 0.25	5.43	4.19	5.5	5.51 $\pm$ 0.80	7.56	16.33	21.54	31.52 $\pm$ 12.70	0.6887
CE5SIM-11	3.05	3.94	6.04	4.61 $\pm$ 1.30	1.51	0.53	2.65	3.03 $\pm$ 1.60	35.51	46.2	47.39	37.74 $\pm$ 0.76	0.6406
CE5SIM-12	6.75	7.42	8.15	7.09 $\pm$ 1.08	4.42	4.49	6.21	6.82 $\pm$ 1.11	8.83	11.94	26.03	22.18 $\pm$ 0.62	0.7208
CE5SIM-13	–	–	–	6.42 $\pm$ 1.28	–	–	–	7.44 $\pm$ 4.26	–	–	–	78.88 $\pm$ 26.69	0.7193

Note. Fitting parameters were used to calculate  $(a - b)$  with standard deviation except for experiment number CE5SIM-13, where three velocity steps showed significant stick-slip and where  $(a - b)$  values were calculated using the velocity step method. There were six velocity steps in each set of experiments, with the first velocity step discarded for each set of experiments because it was not at steady state.

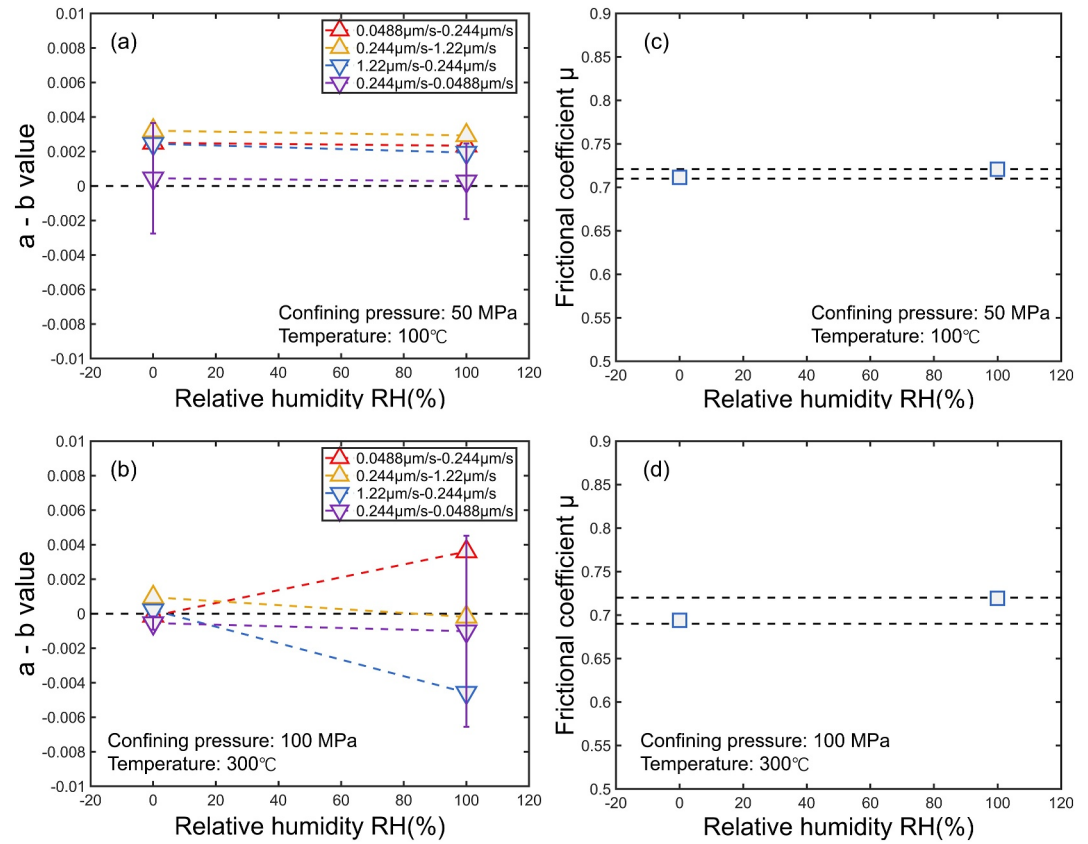
### 3. Results

A total of 13 sets of experiments were performed to investigate the effects of stress, temperature, and relative humidity on the frictional properties of the synthetic gouges (Table 1, Text S1, Figures S4–S6, and Table S3 in Supporting Information S1). Based on the temperature profile of the lunar interior derived from the previous work, we set up experiments at four representative temperatures: 100, 200, 300, and 450°C and confining pressures of 25, 50, 75, and 100 MPa with outliers to 200 MPa (Table S2 in Supporting Information S1). These idealized confining pressure conditions are used to explore the frictional properties of lunar faults at different depths (Table S4 in Supporting Information S1).

At a confining pressure of 25 MPa, we observed a transition of the velocity dependence of the fault gouges from velocity-strengthening behavior at 100°C to velocity-weakening behavior at 200°C to then velocity-strengthening behavior at 450°C ( $a - b = -0.00161 \sim 0.00492$ ) (accompanied by a relatively large standard deviation (Figure 3a)). We observed a similar pattern at 100 MPa when the velocity dependence of the fault gouge exhibited velocity-neutral behavior at 200 and 300°C (Figure 3b). The velocity dependence of the synthetic gouges was not significantly correlated with the stress state. The velocity dependence of the fault gouges does not change significantly ( $a - b = 0.00021 \sim 0.00492$ ) over the entire range of 25–200 MPa (Figure 3c). Under nominal dry conditions, the frictional strength of the simulated fault generally decreased with increasing stress state but did not



**Figure 3.** Frictional coefficient  $\mu$  and frictional stability parameter ( $a - b$ ) for synthetic gouges under dry conditions. Values of ( $a - b$ ) versus (a) temperature at 25 MPa and (b) temperature at 100 MPa; values of ( $a - b$ ) versus (c) confining pressure at 100 °C; frictional coefficient  $\mu$  versus (d) temperature at 25 MPa and (e) temperature at 100 MPa; frictional coefficient  $\mu$  versus (f) confining pressure at 100 °C. Among the various environmental parameters, temperature conditions dominate the velocity dependence of the basaltic faults and stress conditions dominate their strength.



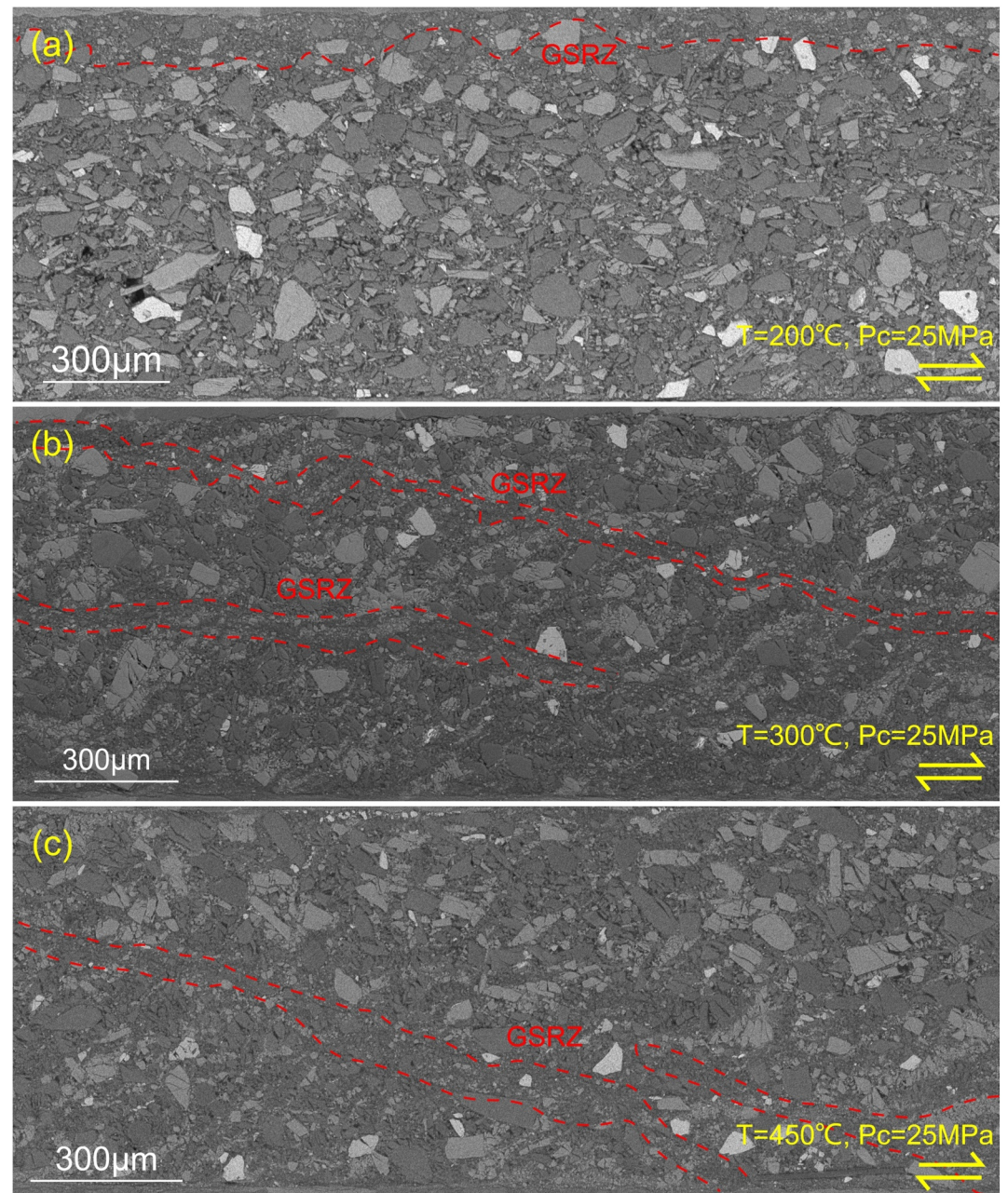
**Figure 4.** Frictional coefficient  $\mu$  and frictional stability ( $a - b$ ) for synthetic gouges under varied experimental conditions. Values of ( $a - b$ ) versus relative humidity RH at (a) relatively low confining pressure–temperature and (b) relatively high confining pressure–temperature; frictional coefficient  $\mu$  versus relative humidity RH at (c) relatively low confining pressure–temperature and (d) relatively high confining pressure–temperature.

show significant changes with temperature. The range of friction strengths at 25 and 100 MPa are 0.7123–0.7298 and 0.6715–0.6946, respectively (Figures 3d and 3e), but show a decrease from 0.7298 at 25 MPa to 0.6406 at 200 MPa at 100°C (Figure 3f). The correspondence between the projected depth, effective normal stress, and stress drop of the fault is shown in Table S4 in Supporting Information S1.

To further analyze the unique properties of the dry gouge and provide insights into possible differences between earthquakes and shallow moonquakes, we supplemented two wet experiments for comparison with the dry experiments. In high-temperature-stress water-saturated experiments, the fault gouge exhibited velocity-weakening behavior at higher velocities and velocity-strengthening behavior at lower velocities (Figure 4b). In contrast, this difference is not apparent for low-temperature-stress conditions (Figure 4a). Both experiments conducted in saturated conditions show higher frictional strength than the nominal dry state (Figures 4c and 4d). Results for the effects of humidity on frictional stability demonstrate that the velocity dependence of gouges under higher temperature-stress is more relevant to slip velocity. Stick-slip occurs at higher velocity while gouge shows stable slip at lower velocity. Conversely, the similarity between the velocity dependences shows that humidity has no impact on frictional stability at a lower temperature and stress.

Microstructural observations demonstrate that the gouges sheared at 25 MPa develop a grain size reduction zone (GSRZ) without any apparent Riedel shear zone (Figure 5). These grain size reduction zones comprised cataclastic flow parallel to the shearing direction at 200°C and deviated at 300 and 450°C. As temperature increases, particles in the bulk become progressively more shattered and create finer particles. At 200 MPa, the microstructure exhibits more Riedel shear zones and boundary shear zones accompanied by ductile deformations relative to that at 100 MPa (Figure 6). Ductile deformation refers to comminuted particle flow in the shear orientation or the plastic deformation of the particles, with such deformation absorbing the shear strain and





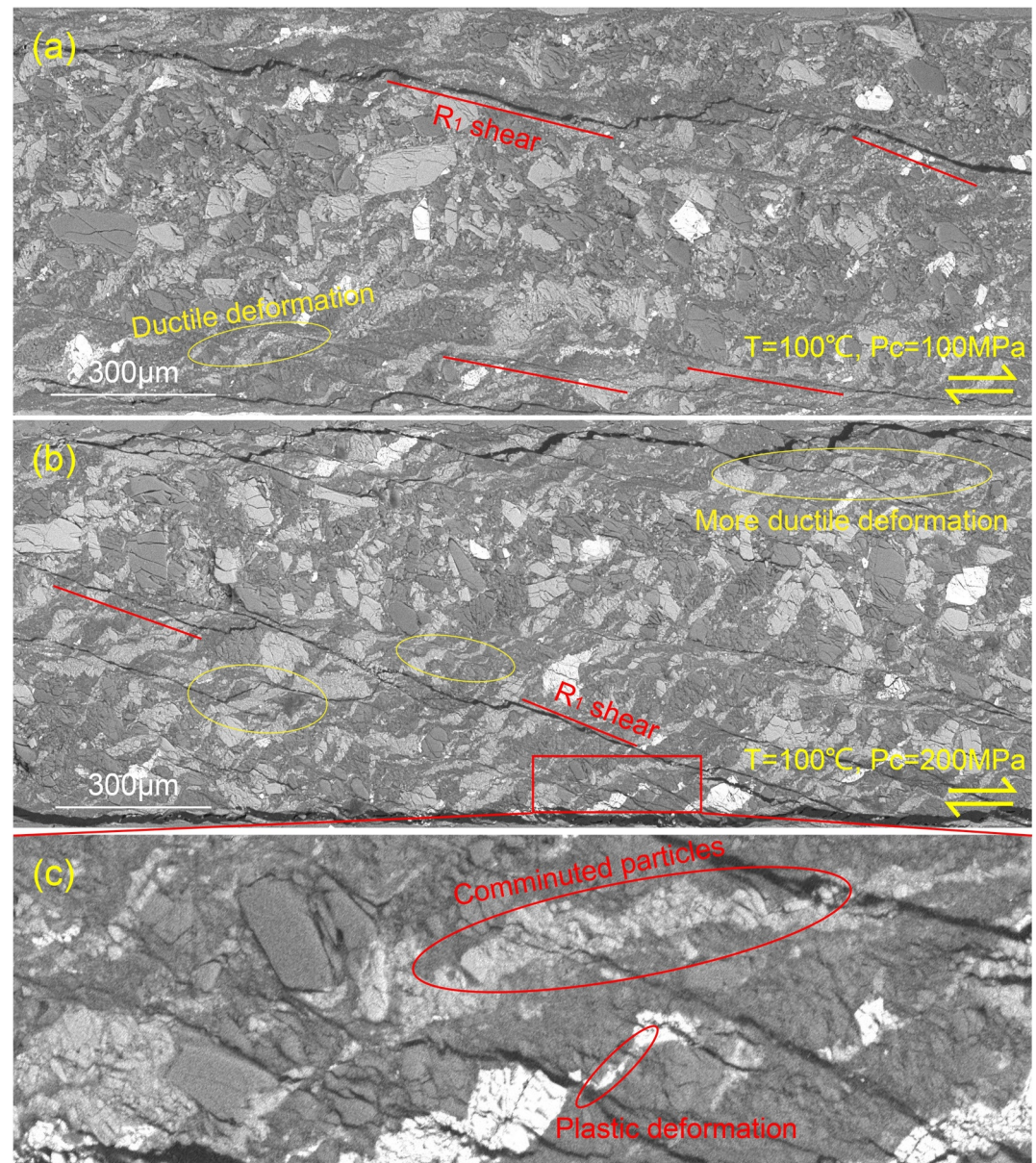
**Figure 5.** Microstructural images for experiments CE5SIM-2, CE5SIM-3, and CE5SIM-4; From panels (a–c), the grain size reduction zone located in the boundary of the gouges transfers to the Riedel shear zone.

inhibiting the sliding of the localized shear zone. In these cases, the dilation and compaction effects in the fault gouge compete to dominate the frictional behavior (Zhang & He, 2016). The microscopic results of the two effects and their implications for the frictional response will be fully discussed in the next section.

## 4. Discussion

### 4.1. The Implication of Gouge Rheologic Characteristics for Shallow Moonquakes

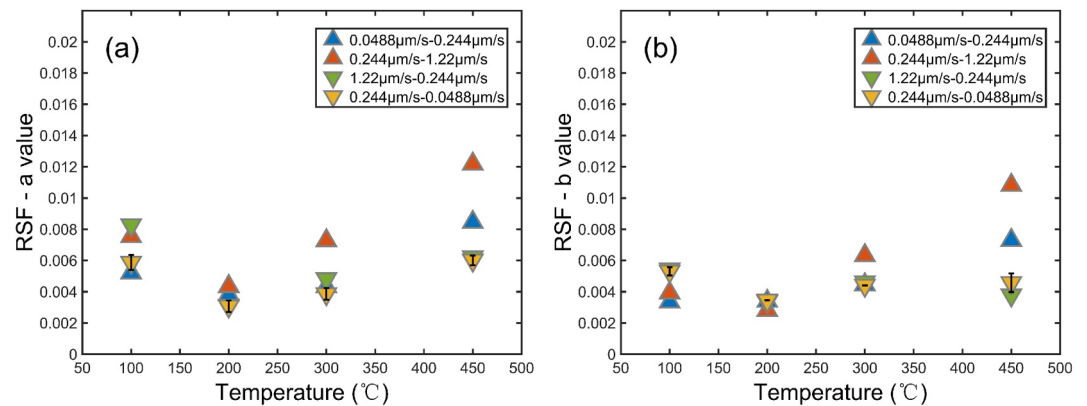
The presence of native anorthosite and basalt determines the seismic potential in the lunar crust. The friction and stability results for the synthetic gouges show the potential instability of basaltic faults over a range of depths and corresponding temperatures. The frictional strength that decreases with increasing confining pressure ( $\mu$  from



**Figure 6.** Microstructural images for experiments CE5SIM-5 and CE5SIM-11; From panels (a, b), gouges show more Riedel shear zones and ductile deformations. (c) Zoomed-in view of the red box in panel (b): Mineral elongation is related to the flow of comminuted particles as well as the plastic deformation of the particles.

0.73 to 0.64) is not sensitive to temperature variation ( $\mu \sim 0.7$ ), implying that basaltic faults might be more readily reactivated at greater depths. In addition, frictional stability shows a trend that decreases first and then increases with increasing temperature—similar to that previously observed for gabbro and clay—indicating the important role of temperature in controlling the frictional properties (Den Hartog et al., 2012; Den Hartog & Spiers, 2014; He et al., 2006; Mitchell et al., 2015; Niemeijer & Spiers, 2007).

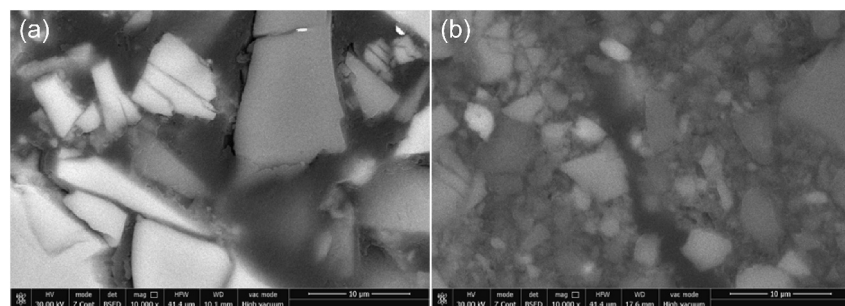
An interesting phenomenon in our results is that the direct ( $a$  value) and evolution effects ( $b$  value) of the RSF parameters show a similar trend to that of  $a - b$  values (Figures 3b and 7) with temperature. Generally,  $a$  and  $b$  values exhibit opposite evolutionary trends, or large changes in one of them are more likely to contribute to the switch between velocity-strengthening and velocity-weakening behaviors (Barbot, 2022; Mitchell et al., 2015). The  $a$  values evolve in relation to any velocity-dependent process in shear. Conversely,  $b$  values evolve by mechanisms related to phenomena such as plastic flow, structural evolution, and pressure solution (He



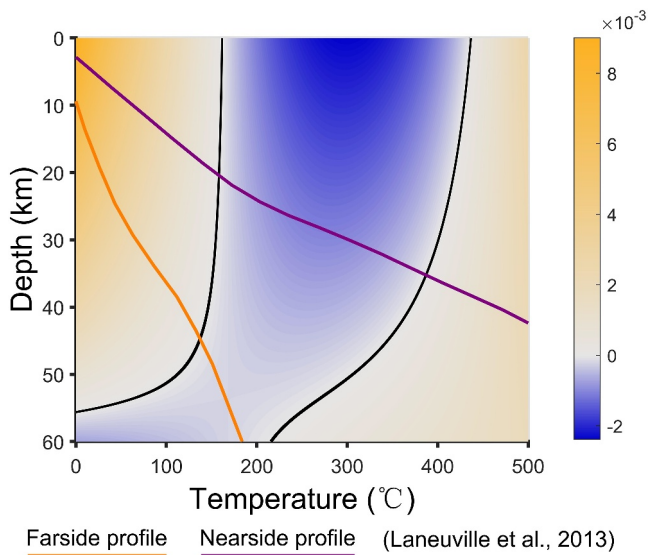
**Figure 7.** Evolution of friction parameters  $a$  (panel a) and  $b$  (panel b) with temperature at 100 MPa.

et al., 2016). Other mechanisms, such as flash heating, have been proposed to directly explain the dynamic weakening of fault strength (Rice, 2006). In our dry experiments, only brittle fracturing and ductile deformation are present. Despite the presence of small amounts of bound water in real lunar soils, experimental results show that pressure solution and plastic flow are negligible or even absent during the creep of faults since the change in  $b$  values is not significant relative to  $a$  values. In contrast, structural evolution can adequately explain the similarity between the evolution patterns of the  $a$  and  $b$  values. The reasons are as follows: (a). The direct effect caused by the velocity change is a prerequisite for the evolution effect to occur. (b). The similarity between  $a$  and  $b$  values suggests that velocity-dependent processes may also dominate the evolution effect. This potentially contributes to the same pattern in the variation in fault stability  $a - b$  caused by the difference in the relative magnitudes of  $a$  and  $b$  values due to the shear localization and structural evolution.

Temperature and stress effects are not directly manifested in the grain morphology and structural characteristics of the fault gouge. Distinguishing the results from pure plagioclase (He et al., 2016), basalts contain a variety of minerals. The rheological properties of these minerals may control the structural evolution of the fault. In the case of the main components, plagioclase and pyroxene, the flow stress of pyroxene is several times higher than that of plagioclase for the same strain rate at lower differential stresses (<120 MPa) and temperatures (<1,100 K), and the ratio of the differential stresses decreases as the temperature increases (Bystricky & Mackwell, 2001; Rybacki & Dresen, 2000). In addition, the results of friction experiments at low confining pressure (60 MPa) indicate that mineral heterogeneity significantly reduces the frictional strength of the faults and makes them more unstable (Bedford et al., 2022). Thus, the deformation of the mineral fragments in the basaltic gouge is heterogeneous during shearing, which may result in variation in the frictional stability of the fault under different temperature-stress conditions. Based on the above, unstable sliding of the dry synthetic fault gouge may be explained by the microphysical model of quartz proposed by Bedford and Faulkner (2021). At a confining pressure of  $\sim 25$  MPa, fault gouges at a shear strain of  $\sim 3.6$  (Figure 5) at 200°C develop an initial R-shear zone that gradually converts to an inconspicuous Y-shear zone. The thin layer of grain size reduction implies that the shear strain is focused in the shear band (Figure 5a). In contrast, as the temperature increased to 300 and 450°C (Figures 5b and 5c), the GSRZ



**Figure 8.** Microstructural images under (a) 200°C and (b) 450°C; At 200°C, the bulk of the fault gouge exhibits brittle fractures of larger particles, but at 450°C, it exhibits more cataclastic flow.



**Figure 9.** Frictional instability for lunar basaltic faults, indicated by  $(a - b)$  values, as a function of depth and temperature. The color bar indicates the values of  $(a - b)$ . The reference depth of 60 km refers to the possible maximum thickness of the lunar crust. The black contour line represents the boundary where  $a - b = 0$ . The orange solid line represents the temperature profile of the farside of the Moon, and the purple solid line represents the temperature profile of the nearside of the Moon (Laneuville et al., 2013). These two profiles constrain the depth range of shallow moonquakes and indicate that shallow moonquakes are mechanically feasible in the lunar crust.

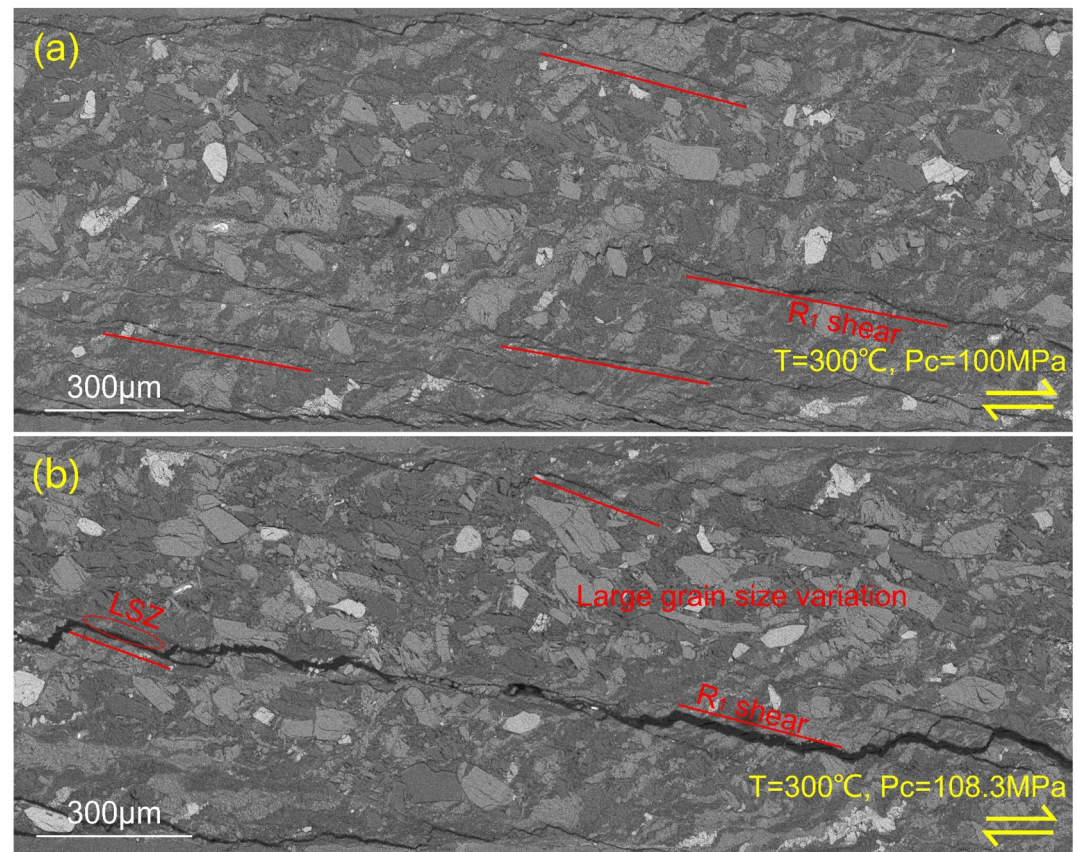
et al., 2012). To further investigate the possible depth of shallow moonquakes and provide a reference for the correctness of different moonquake depth reposition results, we used a parabolic approximation to fit the measured  $(a - b)$  at velocity steps  $0.244 \mu\text{m/s}$ – $0.0488 \mu\text{m/s}$  as functions of temperature at 25 and 100 MPa (Figure S7 in Supporting Information S1). Fitting results imply that potential instability of basaltic faults should occur over the temperature range  $162^\circ\text{C}$ – $429^\circ\text{C}$  at 9.7 km depth and from  $147^\circ\text{C}$  to  $369^\circ\text{C}$  at 40.6 km depth. Combining those two fitting functions by linear interpolation, we obtain a relation defining (lunar) basaltic fault instability, indicated by  $(a - b)$  values, as a function of depth and temperature (Figure 9).

Temperature profiles in the lunar interior are typically obtained through the inversion of data gathered from lunar missions or through the prediction of numerical models, with simplifications involving the division of the Moon into homogeneous layers based on depth (Karato, 2013; Kuskov & Kronrod, 1998). The variety of methods employed allows for the generation of temperature profiles that can explain a wide range of phenomena. For example, two representative temperature profiles from Kuskov and Kronrod (1998) and Karato (2013) are close to the potential brittle-ductile transition temperatures derived from the deep moonquake data set (Kawamura et al., 2017). These temperature distributions demonstrate a superior fit to temperatures in the lunar mantle region, with the caveat that the fit in the shallow crust is inadequate and subject to considerable uncertainty. In this study, we reference temperature profiles from a study based on a thermochemical convection model that predicts the temperature profiles of both the present-day nearside and farside of the Moon (Laneuville et al., 2013). Furthermore, diurnal temperature variations are attenuated in the lunar regolith at depths below  $\sim 1$  m (Heiken et al., 1991; Ran & Wang, 2014). To focus on deeper faults, we have ignored diurnal temperature variations at the lunar surface to focus on deeper faults. Because radiogenic heat sources are not spatially uniform in concentration, the temperature at a given depth in the lunar interior may lie between the values predicted by the nearside and farside temperature profiles as end-member values. In consideration of the global temperatures of the Moon, the model-predicted nearside and farside temperature profiles can be considered as the upper and lower limits of the temperature range, given that the radiative heat source Procellarum KREEP Terrane is situated on the nearside of the Moon (Laneuville et al., 2013). The aforementioned temperature profiles are employed to define the potential depth range for shallow moonquakes. The results indicate that shallow moonquakes may occur at depths of 20–60 km within the lunar crust. Additionally, the depth of these shallow moonquakes appears to be shallower on the

developed within the fault gouge at  $<30^\circ$  in the shear direction. Fine particles in other areas suggest that part of the shear strain is focused in the zone of general shear (Figures 5b and 5c and 8b), in contrast to brittle particle breakage that is distributed throughout the fault at lower temperatures (Figures 5a and 8a).

A similar pattern was observed under 100 MPa, and the microstructures show an apparent boundary shear zone at  $300^\circ\text{C}$  rather than the Riedel shear zone at  $100^\circ\text{C}$ , congruent with the velocity dependence showing a decreasing trend first with increasing temperature (Figures 6a and 10a). Although the gouges exhibit more Riedel shear zones and boundary shear zones under higher confining pressures, which would make the fault prone to velocity-weakening behavior (Logan et al., 1992), more ductile deformation can also be seen that contributes to the velocity-strengthening regime (Figure 6) (Hirauchi et al., 2020). This is consistent with the observation that the velocity dependence shows no apparent variation under different confining pressures (Figure 3c) (Zhang & He, 2016).

Velocity-weakening behaviors exhibited under limited conditions suggest that basaltic faults present in the lunar crust may be sources of shallow moonquakes, which suggests brittle failure as a possible origin (Gillet et al., 2017). But in several lunar models, the seismic depth data show two opposite scenarios, with a portion of the data concentrated above 25 km and another portion of the data below 50 km (Gagnepain-Beyneix et al., 2006; Garcia et al., 2011; Gillet et al., 2017; Khan et al., 2006; Lognonné et al., 2003) (Figure S1 in Supporting Information S1). In general, temperature and stress increase with depth, at which point the deformation mechanism of the rock changes from brittle to ductile regimes (Heap et al., 2022; Violay



**Figure 10.** Microstructural images of experiments CE5SIM-7 and CE5SIM-13; From panel (a, b), gouges show less ductile deformation and larger grain size variation.

nearside compared to the farside of the Moon (Figure 9). Notably, the heterogeneous distribution of radiative heat sources may result in anomalously high temperatures at shallower depths on the nearside of the Moon, which could potentially lead to shallow moonquakes within the 20 km depth range.

#### 4.2. The Differences Between Earthquakes and Moonquakes on Basaltic Faults

In contrast to the Moon, the Earth's crust contains large amounts of free water, and these fluids influence the fault's slip behavior by altering pore pressures and heat release processes as well as mineral replacement within the faults (Dieterich & Conrad, 1984; Violay et al., 2014). The microscopic results show that under dry conditions, high temperature-pressure coupling promotes the development of the Riedel shear zone and boundary shear zone (Figure 10a). In a saturated condition, this behavior is enhanced. It is also accompanied by a significant particle size variation with particles in the gouges, confirming the stick-slip behavior generated by fault gouges at higher velocities (Figure 10b). The dilation effect decreases for the slower slip, and the fault gouge transfers from stick-slip to a stable state. At this condition, particle fragmentation becomes more prevalent and fills shear zones, making shear zones incoherent, and fault gouges exhibit only velocity-strengthening behavior at lower slip velocities (Figure 10b).

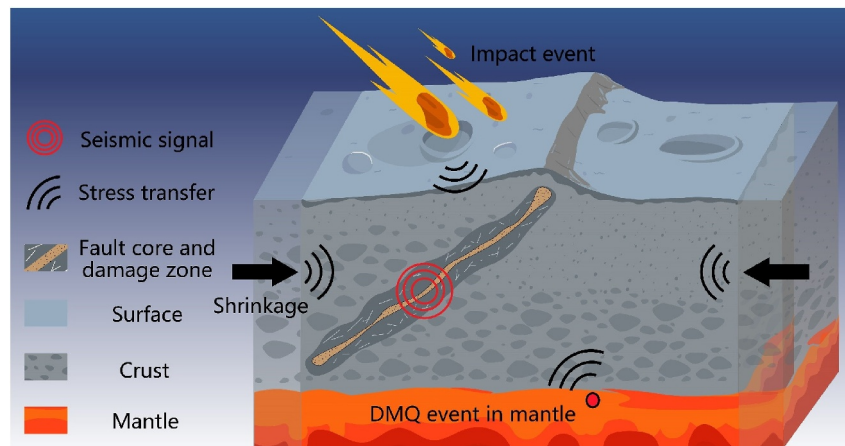
Combined results for humidity effects suggest that the coupling effect of temperature, stress, and humidity controls the mechanical differences between earthquakes and shallow moonquakes on basaltic faults. From the data, it is reasonable to speculate that the thermal effect is one of the factors influencing fault sliding behavior and that when fluids jointly participate in the frictional evolution process, the increase in ductile deformation due to thermal effects lags, thus triggering more violent and unstable sliding (Meyer et al., 2019). These results also shed light on the frictional behavior of basaltic faults in subduction zones as the mineralogical compositions of the CE-5 samples are similar to those of the Earth's oceanic tholeiitic basalts in that both contain significant amounts of feldspar and pyroxene.

### 4.3. Potential Origins of Shallow Moonquakes

Stress drop  $\Delta\tau$ , defined as the difference between shear stress before and after fault rupture, is related to the seismic energy release and an essential parameter for characterizing the behavior of seismic nucleation (Shapiro & Dinske, 2021). Unusually high (up to 210 MPa) stress drops were estimated from lunar seismic data by assuming that the mechanical properties of the shallow moonquakes are the same as earthquakes (Oberst, 1987). In addition, the values of Brune-type stress drops for terrestrial earthquakes of moderate size are usually less than 10 MPa, confirming that the estimated stress drops for some events obtained from seismic observations on the Moon are unusually high but still with moderate magnitudes (Trugman et al., 2017). Laboratory stress drop in our experiments was calculated as the product of effective normal stress and the dimensionless parameter ( $a - b$ ) (Beeler et al., 2001). Our stress drop evaluations from stable sliding are close to the reported dynamic stress drop minimum. Despite the gap between the two types of stress drops, our results may indirectly explain the smaller stress drop events triggered by shear sliding on mature faults that exhibit velocity-weakening behavior, especially since some small magnitude events are not included in the catalog of shallow moonquakes (Hurford et al., 2020). The other class of moonquakes with larger stress drops but moderate magnitudes imply limited nucleation size or a high degree of healing of young faults or that the moonquakes arose from the rupture of the intact lunar crust. When porosity predictions (12%) for the lunar crust are reliable, it is suggested that the lunar bedrock is fragmented and not intact (Wieczorek et al., 2013). Since the medium is not continuous, this will limit the size of seismic nucleation patches. Shallow moonquakes can only nucleate over small areas and immediately scatter continuously over the fractured rock mass, increasing the duration of the seismic wavetrain. In addition, when velocity-weakening faults continue to accelerate or asperities rupture with supershear velocity, then dynamic weakening mechanisms such as flash heating may be triggered, which may be another reason for the large stress drop (Acosta et al., 2018; Passelègue et al., 2013).

Basaltic rocks are present on several other planets, and the dynamic weakening mechanism associated with fluid pressurization can explain the causes of earthquakes but not explain the genesis of moonquakes due to the absence of free water (Chen et al., 2023). Moreover, lunar volcanism has ceased, and metamorphic effects such as thermal contact metamorphism no longer exist, although they may be another reason for altering fault stability and triggering earthquakes (An et al., 2021). Ice-bearing faults on some planets may show phase changes between ice and water in shear that can be explained by flash heating (Lucas et al., 2014). However, for the Moon, where the changes in the rock mass properties are small, flash heating is unlikely to occur until fault slip is sufficiently fast, and the mechanism does not provide an explanation for the acceleration of the fault. Therefore, stress transfer is an important candidate for the triggering mechanism of shallow moonquakes, taking into account the significant influence of the mechanical behavior on the stability of basaltic faults in the lunar crust. Normal stress variations applied to fault zones, well documented on Earth, are typically the result of stress transfer caused by natural seismicity, planetary tides, human activities, and other environmental forcings (Goebel et al., 2016; Ide & Tanaka, 2014). Such stress transfer can directly trigger fault reactivation or indirectly as the result of long-term stress accumulation. In particular, long-term stress accumulation reactivates faults with stress states approaching criticality and thus possibly triggers shallow moonquakes. High stress drop events are likely to occur on locked, discontinuous, or young faults. For the Moon, crustal stresses may evolve as a result of stress transfer from lunar cooling and thermal contraction, tidal attraction, impact events on the lunar surface and deep moonquakes within the lunar mantle. In addition, such normal stress oscillations resulting from the above activities may contribute to the healing of the fault (Richardson & Marone, 1999). Together, stress transfer and concentration originating from these combined processes may factor into the reactivation of basaltic faults and result in shallow moonquakes (Figure 11).

The shallow moonquakes that occur within the lunar crust can be categorized into two types: those initiated on mature faults, where shearing behavior is governed by fault gouge, and those resulting from the rupture of intact lunar crust or the rupture of interlocking asperities on young faults. Our study elucidates that the former type of shallow moonquakes predominantly occurs on basaltic faults. This specificity is attributed to the irregular stress and deformation arising from mineral heterogeneity, leading to unstable sliding. In contrast, on mature plagioclase faults, the direct effect parameter, denoted as  $a$ , increases with temperature within the 100–600°C range. Meanwhile, the evolution effect,  $b$ , remains constant and minimal in relation to the direct effect (He et al., 2016). Pure plagioclase minerals are less prone to uneven stress during the shearing process. Thus, mature plagioclase faults may exhibit velocity-strengthening behaviors ( $a - b > 0$ ) in the range 100–600°C. Considering that true anorthosite has up to 90% plagioclase (Wood et al., 1970), the frictional stability of plagioclase faults can provide



**Figure 11.** Potential mechanisms of shallow moonquakes. DMQ refers to deep moonquake events. Stress from shrinkage is a result of cooling of the lunar interior (Watters et al., 2019). Impact events mainly result from meteorite impacts. The combined and cumulative stress transfer caused by these activities can lead to stress concentrations that fail faults, driving shear reactivation and fault instability under the specific crustal temperature conditions of the Moon.

a reference for true anorthosite or other types of anorthosite with high plagioclase content but is not a quantitative conclusion. In addition, frictional weakening was not observed in another high-velocity friction experiment on anorthosite-bearing gouges under relatively low normal stress conditions, which may provide a reference to the frictional behavior of anorthosite faults (Magnarini et al., 2023). The second type of shallow moonquakes may exist in intact rocks or young faults in both anorthosite and basalt. However, given the Moon's higher porosity, longer evolutionary history, and pre-existing weak structures in the lunar crust, shearing may be more likely to occur on mature faults. Our experiments provide evidence that mature basalt faults (relatively smooth faults with shear behavior controlled by the fault gouge) have the potential to produce shallow moonquakes and confirm that shallow moonquakes may exist in the lunar crust based on our laboratory observations.

## 5. Conclusions

Considering existing significant uncertainties in the prevailing conditions within the lunar crust and seismic localization, our experimental results provide possible mechanisms for the nucleation of shallow moonquakes. Specific conclusions are as follows:

1. No apparent correlations between frictional stability and confining pressure were observed; however, synthetic gouges are shown to display lower frictional strengths at higher confining pressures.
2. A transition for synthetic gouges from velocity-strengthening to velocity-weakening and then back to velocity-strengthening occurs with increasing temperature. This provides the possibility for instability on basaltic faults in the lunar crust – and thus the potential for shallow moonquakes.
3. Differences in the rheological characteristics of basalt mineral fragments dominate the structural evolution of the fault gouge and influence the switch between velocity-strengthening and velocity-weakening behavior. Stress transfer and accumulation by processes such as cooling contraction may trigger the reactivation of velocity-weakening faults and cause shallow moonquakes.

## Data Availability Statement

The processed experimental data for this research are publicly available on Dryad (Zhang et al., 2023).

## References

- Acosta, M., Passelègue, F. X., Schubnel, A., & Violay, M. (2018). Dynamic weakening during earthquakes controlled by fluid thermodynamics. *Nature Communications*, 9(1), 3074. <https://doi.org/10.1038/s41467-018-05603-9>
- An, M., Zhang, F., Min, K. B., Elsworth, D., Marone, C., & He, C. (2021). The potential for low-grade metamorphism to facilitate fault instability in a geothermal reservoir. *Geophysical Research Letters*, 48(11), e2021GL093552. <https://doi.org/10.1029/2021GL093552>
- Barbot, S. (2022). A rate-, state-, and temperature-dependent friction law with competing healing mechanisms. *Journal of Geophysical Research: Solid Earth*, 127(11), e2022JB025106. <https://doi.org/10.1029/2022JB025106>

## Acknowledgments

This research is funded by the National Natural Science Foundation of China (42077247, 42107163), the Fundamental Research Funds for the Central Universities, and the Top Discipline Plan of Shanghai Universities-Class I. DE acknowledges support from the G. Albert Shoemaker endowment. We appreciate the assistance of Changrong He, Wenming Yao, and Shimin Liu in the lab.

- Beard, B. L., Taylor, L. A., Scherer, E. E., Johnson, C. M., & Snyder, G. A. (1998). The source region and melting mineralogy of high-titanium and low-titanium lunar basalts deduced from Lu-Hf isotope data. *Geochimica et Cosmochimica Acta*, 62(3), 525–544. [https://doi.org/10.1016/S0016-7037\(97\)00373-6](https://doi.org/10.1016/S0016-7037(97)00373-6)
- Bedford, J. D., & Faulkner, D. R. (2021). The role of grain size and effective normal stress on localization and the frictional stability of simulated quartz gouge. *Geophysical Research Letters*, 48(7), e2020GL092023. <https://doi.org/10.1029/2020GL092023>
- Bedford, J. D., Faulkner, D. R., & Lapusta, N. (2022). Fault rock heterogeneity can produce fault weakness and reduce fault stability. *Nature Communications*, 13(1), 326. <https://doi.org/10.1038/s41467-022-27998-2>
- Beeler, N. M., Hickman, S. H., & Wong, T. F. (2001). Earthquake stress drop and laboratory-inferred interseismic strength recovery. *Journal of Geophysical Research*, 106(B12), 30701–30713. <https://doi.org/10.1029/2000jb900242>
- Bystricky, M., & Mackwell, S. (2001). Creep of dry clinopyroxene aggregates. *Journal of Geophysical Research*, 106(B7), 13443–13454. <https://doi.org/10.1029/2001JB000333>
- Chen, J., Hunfeld, L. B., Niemeijer, A. R., & Spiers, C. J. (2023). Fault weakening during short seismic slip pulse experiments: The role of pressurized water and implications for induced earthquakes in the Groningen gas field. *Journal of Geophysical Research: Solid Earth*, 128(2), e2022JB025729. <https://doi.org/10.1029/2022JB025729>
- Crawford, I. A., & Joy, K. H. (2014). Lunar exploration: Opening a window into the history and evolution of the inner Solar System. *Philosophical Transactions of the Royal Society A: Mathematical, Physical & Engineering Sciences*, 372(2024), 20130315. <https://doi.org/10.1098/rsta.2013.0315>
- Den Hartog, S. A. M., Niemeijer, A. R., & Spiers, C. J. (2012). New constraints on megathrust slip stability under subduction zone P-T conditions. *Earth and Planetary Science Letters*, 353–354, 240–252. <https://doi.org/10.1016/j.epsl.2012.08.022>
- Den Hartog, S. A. M., & Spiers, C. J. (2014). A microphysical model for fault gouge friction applied to subduction megathrusts. *Journal of Geophysical Research: Solid Earth*, 119(2), 1510–1529. <https://doi.org/10.1002/2013JB010580>
- Dieterich, J. H. (1978). Time-dependent friction and the mechanics of stick-slip. *Rock Friction and Earthquake Prediction*, 116(4–5), 790–806. <https://doi.org/10.1007/BF00876539>
- Dieterich, J. H., & Conrad, G. (1984). Effect of humidity on time- and velocity-dependent friction in rocks. *Journal of Geophysical Research*, 89(B6), 4196–4202. <https://doi.org/10.1029/JB089iB06p04196>
- Frohlich, C., & Nakamura, Y. (2006). Possible extra-solar-system cause for certain lunar seismic events. *Icarus*, 185(1), 21–28. <https://doi.org/10.1016/j.icarus.2006.07.002>
- Frye, K. M., & Marone, C. (2002). Effect of humidity on granular friction at room temperature. *Journal of Geophysical Research*, 107(B11), ETG 11-1-ETG 11-13. <https://doi.org/10.1029/2001jb000654>
- Gagnepain-Beyneix, J., Lognonné, P., Chenet, H., Lombardi, D., & Spohn, T. (2006). A seismic model of the lunar mantle and constraints on temperature and mineralogy. *Physics of the Earth and Planetary Interiors*, 159(3–4), 140–166. <https://doi.org/10.1016/j.pepi.2006.05.009>
- Garcia, R. F., Gagnepain-Beyneix, J., Chevrot, S., & Lognonné, P. (2011). Very preliminary reference Moon model. *Physics of the Earth and Planetary Interiors*, 188(1–2), 96–113. <https://doi.org/10.1016/j.pepi.2011.06.015>
- Giacomel, P., Ruggieri, R., Scuderi, M. M., Spagnuolo, E., Di Toro, G., & Colletini, C. (2021). Frictional properties of basalt experimental faults and implications for volcano-tectonic settings and geo-energy sites. *Tectonophysics*, 811, 228883. <https://doi.org/10.1016/j.tecto.2021.228883>
- Gillet, K., Margerin, L., Calvet, M., & Monnerieu, M. (2017). Scattering attenuation profile of the Moon: Implications for shallow moonquakes and the structure of the megaregolith. *Physics of the Earth and Planetary Interiors*, 262, 28–40. <https://doi.org/10.1016/j.pepi.2016.11.001>
- Goebel, T. H. W., Hosseini, S. M., Cappa, F., Hauksson, E., Ampuero, J. P., Aminzadeh, F., & Saleeby, J. B. (2016). Wastewater disposal and earthquake swarm activity at the southern end of the Central Valley, California. *Geophysical Research Letters*, 43(3), 1092–1099. <https://doi.org/10.1002/2015GL066948>
- He, C., Tan, W., & Zhang, L. (2016). Comparing dry and wet friction of plagioclase: Implication to the mechanism of frictional evolution effect at hydrothermal conditions. *Journal of Geophysical Research: Solid Earth*, 121(9), 6365–6383. <https://doi.org/10.1002/2016JB012834>
- He, C., Yao, W., Wang, Z., & Zhou, Y. (2006). Strength and stability of frictional sliding of gabbro gouge at elevated temperatures. *Tectonophysics*, 427(1–4), 217–229. <https://doi.org/10.1016/j.tecto.2006.05.023>
- Head, J. W., & Wilson, L. (2017). Generation, ascent and eruption of magma on the Moon: New insights into source depths, magma supply, intrusions and effusive/explosive eruptions (Part 2: Predicted emplacement processes and observations). *Icarus*, 283, 176–223. <https://doi.org/10.1016/j.icarus.2016.05.031>
- Heap, M. J., Meyer, G. G., Noël, C., Wadsworth, F. B., Baud, P., & Violay, M. E. S. (2022). The permeability of porous volcanic rock through the brittle-ductile transition. *Journal of Geophysical Research: Solid Earth*, 127(6), e2022JB024600. <https://doi.org/10.1029/2022JB024600>
- Heiken, G., Vaniman, D., & French, B. M. (1991). *Lunar sourcebook: A user's guide to the Moon*. Cambridge University Press.
- Hirauchi, K. I., Yoshida, Y., Yabe, Y., & Muto, J. (2020). Slow stick-slip failure in halite gouge caused by brittle-plastic fault heterogeneity. *Geochemistry, Geophysics, Geosystems*, 21(9), e2020GC009165. <https://doi.org/10.1029/2020GC009165>
- Hirt, C., & Featherstone, W. E. (2012). A 1.5km-resolution gravity field model of the Moon. *Earth and Planetary Science Letters*, 329–330, 22–30. <https://doi.org/10.1016/j.epsl.2012.02.012>
- Hui, H., Peslier, A. H., Zhang, Y., & Neal, C. R. (2013). Water in lunar anorthosites and evidence for a wet early Moon. *Nature Geoscience*, 6(3), 177–180. <https://doi.org/10.1038/ngeo1735>
- Hurford, T. A., Henning, W. G., Maguire, R., Lekic, V., Schmerr, N., Panning, M., et al. (2020). Seismicity on tidally active solid-surface worlds. *Icarus*, 338, 113466. <https://doi.org/10.1016/j.icarus.2019.113466>
- Ide, S., & Tanaka, Y. (2014). Controls on plate motion by oscillating tidal stress: Evidence from deep tremors in western Japan. *Geophysical Research Letters*, 41(11), 3842–3850. <https://doi.org/10.1002/2014GL060035>
- Ikari, M. J., Marone, C., & Saffer, D. M. (2011). On the relation between fault strength and frictional stability. *Geology*, 39(1), 83–86. <https://doi.org/10.1130/G31416.1>
- Ikari, M. J., Wilckens, F. K., & Saffer, D. M. (2020). Implications of basement rock alteration in the Nankai Trough, Japan for subduction megathrust slip behavior. *Tectonophysics*, 774, 228275. <https://doi.org/10.1016/j.tecto.2019.228275>
- Ito, Y., Obara, K., Shiomi, K., Sekine, S., & Hirose, H. (2007). Slow earthquakes coincident with episodic tremors and slow slip events. *Science*, 315(5811), 503–506. <https://doi.org/10.1126/science.1134454>
- Karato, S. I. (2013). Geophysical constraints on the water content of the lunar mantle and its implications for the origin of the Moon. *Earth and Planetary Science Letters*, 384, 144–153. <https://doi.org/10.1016/j.epsl.2013.10.001>
- Kawamura, T., Lognonné, P., Nishikawa, Y., & Tanaka, S. (2017). Evaluation of deep moonquake source parameters: Implication for fault characteristics and thermal state. *Journal of Geophysical Research: Planets*, 122(7), 1487–1504. <https://doi.org/10.1002/2016JE005147>



- Khan, A., MacLennan, J., Taylor, S. R., & Connolly, J. A. D. (2006). Are the Earth and the Moon compositionally alike? Inferences on lunar composition and implications for lunar origin and evolution from geophysical modeling. *Journal of Geophysical Research*, *111*(5), E05005. <https://doi.org/10.1029/2005JE002608>
- Kuskov, O. L., & Kronrod, V. A. (1998). Constitution of the Moon: 5. Constraints on composition, density, temperature, and radius of a core. *Physics of the Earth and Planetary Interiors*, *107*(4), 285–306. [https://doi.org/10.1016/S0031-9201\(98\)00082-X](https://doi.org/10.1016/S0031-9201(98)00082-X)
- Lammlein, D. R. (1977). Lunar seismicity and tectonics. *Physics of the Earth and Planetary Interiors*, *14*(3), 224–273. [https://doi.org/10.1016/0031-9201\(77\)90175-3](https://doi.org/10.1016/0031-9201(77)90175-3)
- Laneuville, M., Wieczorek, M. A., Breuer, D., & Tosi, N. (2013). Asymmetric thermal evolution of the Moon. *Journal of Geophysical Research: Planets*, *118*(7), 1435–1452. <https://doi.org/10.1002/jgre.20103>
- Li, C., Hu, H., Yang, M. F., Pei, Z. Y., Zhou, Q., Ren, X., et al. (2022). Characteristics of the lunar samples returned by the Chang'E-5 mission. *National Science Review*, *9*(2), nwab188. <https://doi.org/10.1093/nsr/nwab188>
- Lin, H., Li, S., Xu, R., Liu, Y., Wu, X., Yang, W., et al. (2022). In situ detection of water on the Moon by the Chang'E-5 lander. *Science Advances*, *8*(1), eabl9174. <https://doi.org/10.1126/sciadv.abl9174>
- Lin, Y., Tronche, E. J., Steenstra, E. S., & Van Westrenen, W. (2017). Evidence for an early wet Moon from experimental crystallization of the lunar magma ocean. *Nature Geoscience*, *10*(1), 14–18. <https://doi.org/10.1038/ngeo2845>
- Logan, J. M., Dengo, C. A., Higgs, N. G., & Wang, Z. Z. (1992). Fabrics of experimental fault zones: Their development and relationship to mechanical behavior. *International Geophysics*, *51*, 33–67. [https://doi.org/10.1016/S0074-6142\(08\)62814-4](https://doi.org/10.1016/S0074-6142(08)62814-4)
- Lognonné, P., Gagnepain-Beyneix, J., & Chenet, H. (2003). A new seismic model of the Moon: Implications for structure, thermal evolution and formation of the Moon. *Earth and Planetary Science Letters*, *211*(1–2), 27–44. [https://doi.org/10.1016/S0012-821X\(03\)00172-9](https://doi.org/10.1016/S0012-821X(03)00172-9)
- Lucas, A., Mangeney, A., & Ampuero, J. P. (2014). Frictional velocity-weakening in landslides on Earth and on other planetary bodies. *Nature Communications*, *5*(1), 3417. <https://doi.org/10.1038/ncomms4417>
- Magnarini, G., Aretusini, S., Mitchell, T. M., Pennacchioni, G., Di Toro, G., & Schmitt, H. H. (2023). Friction experiments on lunar analogue gouges and implications for the mechanism of the Apollo 17 long runout landslide. *Journal of Geophysical Research: Planets*, *128*(6), e2022JE007520. <https://doi.org/10.1029/2022JE007520>
- Marone, C., Raleigh, C. B., & Scholz, C. H. (1990). Frictional behavior and constitutive modeling of simulated fault gouge. *Journal of Geophysical Research*, *95*(B5), 7007–7025. <https://doi.org/10.1029/JB095iB05p07007>
- Meyer, G. G., Brantut, N., Mitchell, T. M., & Meredith, P. G. (2019). Fault reactivation and strain partitioning across the brittle-ductile transition. *Geology*, *47*(12), 1127–1130. <https://doi.org/10.1130/G46516.1>
- Mitchell, E. K., Fialko, Y., & Brown, K. M. (2015). Frictional properties of gabbro at conditions corresponding to slow slip events in subduction zones. *Geochemistry, Geophysics, Geosystems*, *16*(11), 4006–4020. <https://doi.org/10.1002/2015GC006093>
- Moriarty, D. P., Dygert, N., Valencia, S. N., Watkins, R. N., & Petro, N. E. (2021). The search for lunar mantle rocks exposed on the surface of the Moon. *Nature Communications*, *12*(1), 1–11. <https://doi.org/10.1038/s41467-021-24626-3>
- Nakamura, Y. (1980). Shallow moonquakes: Are they comparable to earthquakes? In *Lunar and planetary science conference, 11th, Houston, TX, March 17-21, 1980, Proceedings* (Vol. 3, pp. 1847–1853). Pergamon Press.
- Nakamura, Y., Latham, G. V., & Dorman, H. J. (1982). Apollo lunar seismic experiment—Final summary. *Journal of Geophysical Research*, *87*(S01), A117–A123. <https://doi.org/10.1029/jb087is01p0a117>
- Nakamura, Y., Latham, G. V., Dorman, H. J., Ibrahim, A. B., Koyama, J., & Horvath, P. (1979). Shallow moonquakes—depth, distribution and implications as to the present state of the lunar interior. In *Lunar and planetary science conference, 10th, Houston, Tex., March 19-23, 1979, Proceedings* (Vol. 3, pp. 2299–2309). Pergamon Press, Inc.
- Niemeijer, A. R., & Spiers, C. J. (2007). A microphysical model for strong velocity weakening in phyllosilicate-bearing fault gouges. *Journal of Geophysical Research*, *112*(10). <https://doi.org/10.1029/2007JB005008>
- Nunn, C., Garcia, R. F., Nakamura, Y., Marusiak, A. G., Kawamura, T., Sun, D., et al. (2020). Lunar seismology: A data and instrumentation review. *Space Science Reviews*, *216*(5), 89. <https://doi.org/10.1007/s11214-020-00709-3>
- Oberst, J. (1987). Unusually high stress drops associated with shallow moonquakes. *Journal of Geophysical Research*, *92*(B2), 1397–1405. <https://doi.org/10.1029/JB092iB02p01397>
- Passelègue, F. X., Schubnel, A., Nielsen, S., Bhat, H. S., & Madariaga, R. (2013). From sub-Rayleigh to supershear ruptures during stick-slip experiments on crustal rocks. *Science*, *340*(6137), 1208–1211. <https://doi.org/10.1126/science.1235637>
- Phillips, N. J., Belzer, B., French, M. E., Rowe, C. D., & Ujiie, K. (2020). Frictional strengths of subduction thrust rocks in the region of shallow slow earthquakes. *Journal of Geophysical Research: Solid Earth*, *125*(3), e2019JB018888. <https://doi.org/10.1029/2019JB018888>
- Qian, Y., Xiao, L., Head, J. W., van der Bogert, C. H., Hiesinger, H., & Wilson, L. (2021). Young lunar mare basalts in the Chang'e-5 sample return region, northern Oceanus Procellarum. *Earth and Planetary Science Letters*, *555*, 116702. <https://doi.org/10.1016/j.epsl.2020.116702>
- Ran, Z., & Wang, Z. Z. (2014). Simulations of lunar equatorial regolith temperature profile based on measurements of diviner on Lunar Reconnaissance Orbiter. *Science China Earth Sciences*, *57*(9), 2232–2241. <https://doi.org/10.1007/s11430-014-4886-4>
- Rempe, M., Smith, S. A., Ferri, F., Mitchell, T. M., & Di Toro, G. (2014). Clast-cortex aggregates in experimental and natural calcite-bearing fault zones. *Journal of Structural Geology*, *68*, 142–157. <https://doi.org/10.1016/j.jsg.2014.09.007>
- Rice, J. R. (2006). Heating and weakening of faults during earthquake slip. *Journal of Geophysical Research*, *111*(B5), B05311. <https://doi.org/10.1029/2005JB004006>
- Richardson, E., & Marone, C. (1999). Effects of normal stress vibrations on frictional healing. *Journal of Geophysical Research*, *104*(B12), 28859–28878. <https://doi.org/10.1029/1999jb900320>
- Ruina, A. (1983). Slip instability and state variable friction laws. *Journal of Geophysical Research*, *88*(B12), 10359–10370. <https://doi.org/10.1029/JB088iB12p10359>
- Rybacki, E., & Dresen, G. (2000). Dislocation and diffusion creep of synthetic anorthite aggregates. *Journal of Geophysical Research*, *105*(B11), 26017–26036. <https://doi.org/10.1029/2000JB900223>
- Shapiro, S. A., & Dinske, C. (2021). Stress drop, seismogenic index and fault cohesion of fluid-induced earthquakes. *Rock Mechanics and Rock Engineering*, *54*(10), 5483–5492. <https://doi.org/10.1007/s00603-021-0420-3>
- Skarbek, R. M., & Savage, H. M. (2019). RSFit3000: A MATLAB GUI-based program for determining rate and state frictional parameters from experimental data. *Geosphere*, *15*(5), 1665–1676. <https://doi.org/10.1130/GES02122.1>
- Trugman, D. T., Dougherty, S. L., Cochran, E. S., & Shearer, P. M. (2017). Source spectral properties of small to moderate earthquakes in southern Kansas. *Journal of Geophysical Research: Solid Earth*, *122*(10), 8021–8034. <https://doi.org/10.1002/2017JB014649>
- Violay, M., Gibert, B., Mainprice, D., Evans, B., Dautria, J. M., Azais, P., & Pezard, P. (2012). An experimental study of the brittle-ductile transition of basalt at oceanic crust pressure and temperature conditions. *Journal of Geophysical Research*, *117*(B3). <https://doi.org/10.1029/2011JB008884>

- Violay, M., Nielsen, S., Gibert, B., Spagnuolo, E., Cavallo, A., Azais, P., et al. (2014). Effect of water on the frictional behavior of cohesive rocks during earthquakes. *Geology*, *42*(1), 27–30. <https://doi.org/10.1130/G34916.1>
- Watters, T. R., Weber, R. C., Collins, G. C., Howley, I. J., Schmerr, N. C., & Johnson, C. L. (2019). Shallow seismic activity and young thrust faults on the Moon. *Nature Geoscience*, *12*(6), 411–417. <https://doi.org/10.1038/s41561-019-0362-2>
- Weber, R. C., Bills, B. G., & Johnson, C. L. (2009). Constraints on deep moonquake focal mechanisms through analyses of tidal stress. *Journal of Geophysical Research*, *114*(5). <https://doi.org/10.1029/2008JE003286>
- Wieczorek, M. A., Jolliff, B. L., Khan, A., Pritchard, M. E., Weiss, B. P., Williams, J. G., et al. (2006). The constitution and structure of the Lunar interior. *Reviews in Mineralogy and Geochemistry*, *60*(1), 221–364. <https://doi.org/10.2138/rmg.2006.60.3>
- Wieczorek, M. A., Neumann, G. A., Nimmo, F., Kiefer, W. S., Taylor, G. J., Melosh, H. J., et al. (2013). The crust of the Moon as seen by GRAIL. *Science*, *339*(6120), 671–675. <https://doi.org/10.1126/science.1231530>
- Wilson, L., & Head, J. W. (2017). Generation, ascent and eruption of magma on the Moon: New insights into source depths, magma supply, intrusions and effusive/explosive eruptions (Part 1: Theory). *Icarus*, *283*, 146–175. <https://doi.org/10.1016/j.icarus.2015.12.039>
- Wood, J. A., Dickey Jr, J. S., Marvin, U. B., & Powell, B. N. (1970). Lunar anorthosites. *Science*, *167*(3918), 602–604. <https://doi.org/10.1126/science.167.3918.602>
- Zhang, F., Zhao, W., An, M., Shen, X., Tang, J., Zhao, L., et al. (2023). Data from: Shallow moonquake mechanisms illuminated by rheologic characteristics of basaltic gouges [Dataset]. *Dryad*. <https://doi.org/10.5061/dryad.18931zd3b>
- Zhang, L., & He, C. (2016). Frictional properties of phyllosilicate-rich mylonite and conditions for the brittle-ductile transition. *Journal of Geophysical Research: Solid Earth*, *121*(4), 3017–3047. <https://doi.org/10.1002/2015JB012489>
- Zhang, L., He, C., Liu, Y., & Lin, J. (2017). Frictional properties of the South China Sea oceanic basalt and implications for strength of the Manila subduction seismogenic zone. *Marine Geology*, *394*(May), 16–29. <https://doi.org/10.1016/j.margeo.2017.05.006>
- Zuber, M. T., Smith, D. E., Watkins, M. M., Asmar, S. W., Konopliv, A. S., Lemoine, F. G., et al. (2013). Gravity field of the moon from the gravity recovery and interior laboratory (GRAIL) mission. *Science*, *339*(6120), 668–671. <https://doi.org/10.1126/science.1231507>